Supplemental information

Combinatorial immune refocusing within

the influenza hemagglutinin RBD

improves cross-neutralizing antibody responses

Annie Dosey, Daniel Ellis, Seyhan Boyoglu-Barnum, Hubza Syeda, Mason Saunders, Michael J. Watson, John C. Kraft, Minh N. Pham, Miklos Guttman, Kelly K. Lee, Masaru Kanekiyo, and Neil P. King
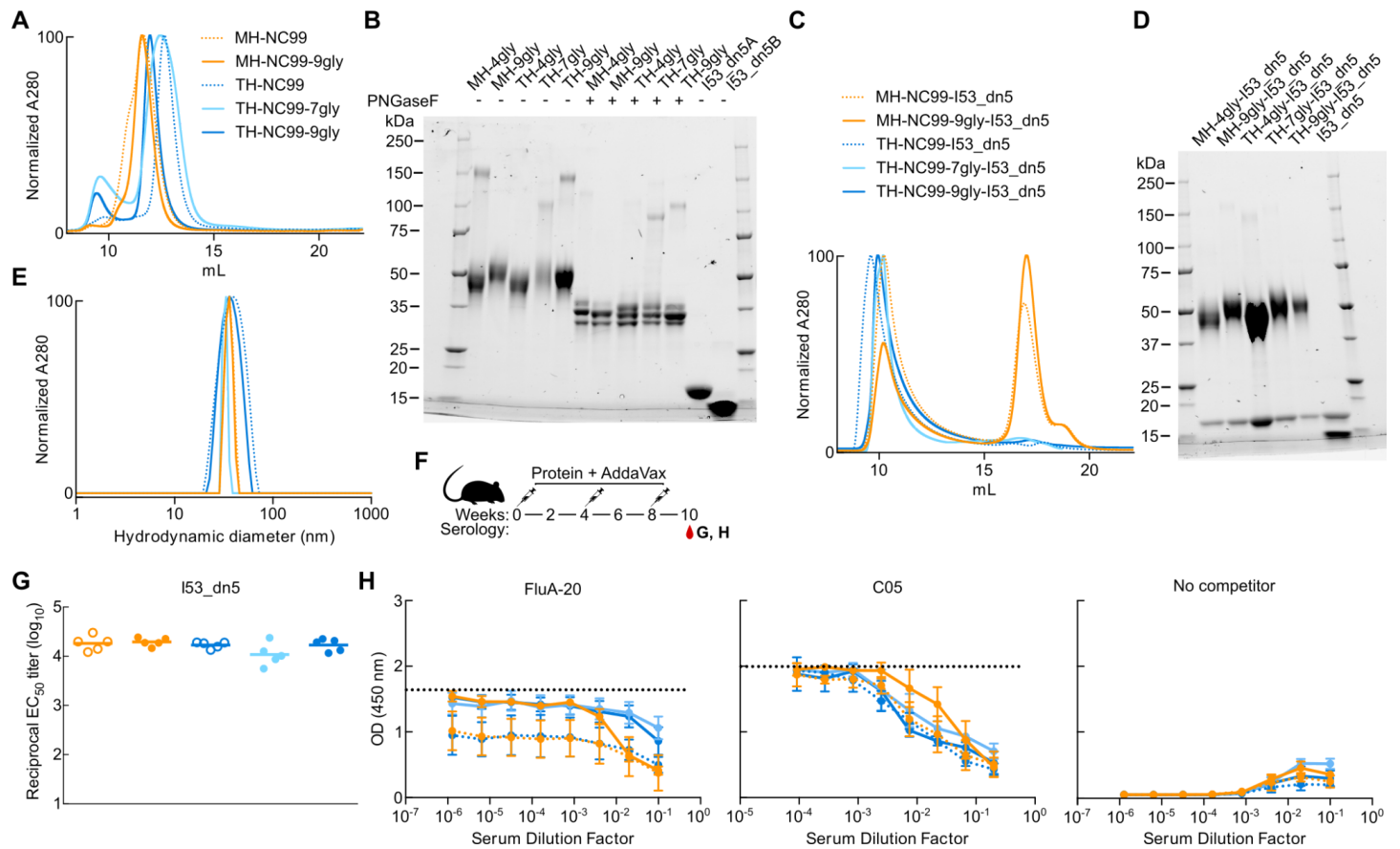
SUPPLEMENTARY FIGURES

Figure S1 Hyperglycosylated TH-NC99-I53_dn5 Mouse Study, Related to Figure 1.

(A) SEC chromatograms of NC99 trihead nanoparticle components on a Superdex 200 Increase 10/300 GL column.

(B) Reducing SDS-PAGE of wild-type and hyperglycosylated NC99 monoheads and trihead components without and with PNGaseF digestion, as well as bare I53_dn5B and I53_dn5A nanoparticle components.

(C) NC99 trihead-I53_dn5 nanoparticle legend for Figures S1C, S1E, S1G, and S1H. SEC chromatograms of NC99 trihead-I53_dn5 nanoparticle immunogens on a Superose 6 Increase 10/300 GL column.

(D) Reducing SDS-PAGE of NC99 trihead-I53_dn5 nanoparticles, as well as the bare I53_dn5 nanoparticle.

(E) DLS of NC99 trihead-I53_dn5 nanoparticles.

(F) Schematic illustrating mouse study timeline, immunizations, and serology timepoint.

(G) ELISA binding titers in week 10 serum against the I53_dn5 nanoparticle scaffold. Each symbol represents an individual animal, and the geometric mean of each group is indicated by the bar (n = 5 mice/group).

(H) Competition ELISA curves for NC99-foldon trimer ELISA antigen between week 10 sera and either FluA-20, C05, or a no competitor negative control. Dashed line is positive control of monoclonal binding in absence of sera. Each line and error bar represents the geometric mean and geometric mean SD, respectively, of the absorbance at 450 nm (n = 5 mice/group)

A

Monoheads

Triheads

5J8 vs. TH-SC18
Anti-PR34 vs. TH-PR34
C05 vs. TH-NC99
5J8 vs. TH-MI15
FluA-20 vs. TH-SC18
FluA-20 vs. TH-PR34
FluA-20 vs. TH-NC99
FluA-20 vs. TH-MI15

B

Monoheads

Triheads

C

MH-SC18-I53_dn5B
MH-PR34-I53_dn5B
MH-NC99-I53_dn5B
MH-MI15-I53_dn5B

MH-SC18-6gly-I53_dn5B
MH-PR34-7gly-I53_dn5B
MH-NC99-9gly-I53_dn5B
MH-MI15-6gly-I53_dn5B

TH-SC18-I53_dn5B
TH-PR34-I53_dn5B
TH-NC99-I53_dn5B
TH-MI15-I53_dn5B

TH-SC18-6gly-I53_dn5B
TH-PR34-7gly-I53_dn5B
TH-NC99-9gly-I53_dn5B
TH-MI15-6gly-I53_dn5B

D

TH-SC18-I53_dn5
TH-PR34-I53_dn5
TH-NC99-I53_dn5
TH-MI15-I53_dn5

MH-SC18-I53_dn5
MH-PR34-I53_dn5
MH-NC99-I53_dn5
MH-MI15-I53_dn5

MH-mosaic-I53_dn5
MH-hyperglycosylated-mosaic-I53_dn5
TH-mosaic-I53_dn5
TH-hyperglycosylated-mosaic-I53_dn5
TH-hypervariable-mosaic-I53_dn5

E

F

MH-cocktail-I53_dn5
MH-mosaic-I53_dn5
MH-hyperglycosylated-mosaic-I53_dn5
TH-cocktail-I53_dn5
TH-mosaic-I53_dn5
TH-hyperglycosylated-mosaic-I53_dn5
TH-hypervariable-mosaic-I53_dn5

G

MH-cocktail-I53_dn5 | MH-mosaic-I53_dn5 | MH-hyperglycosylated-mosaic-I53_dn5 | TH-cocktail-I53_dn5 | TH-mosaic-I53_dn5 | TH-hyperglycosylated-mosaic-I53_dn5 | TH-hypervariable-mosaic-I53_dn5
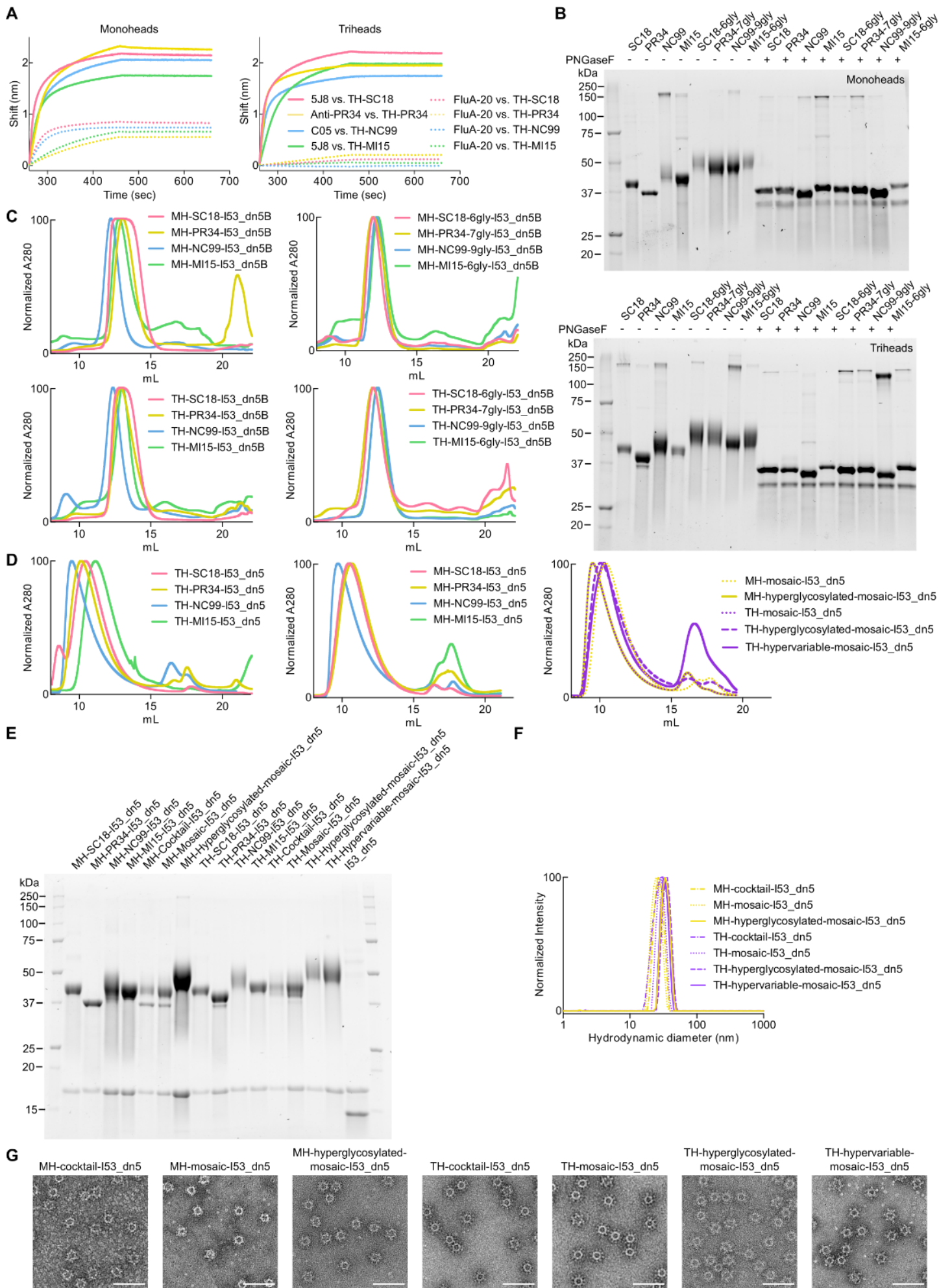
Figure S2 Mosaic, Hyperglycosylated, and Hypervariable Trihead Components and Nanoparticles Purification and Characterization, Related to Figures 2 and 3.

(A) BLI of monohead and trihead nanoparticle components against RBS-directed mAbs (5J8, anti-PR34, and C05) and FluA-20.

(B) Reducing SDS-PAGE of wild-type and hyperglycosylated monohead and trihead nanoparticle components without and with PNGaseF digestion.

(C) SEC chromatograms of wild-type and hyperglycosylated monohead and trihead nanoparticle components on a Superdex 200 Increase 10/300 GL column.

(D) SEC chromatograms of individual H1 strains of monohead- and trihead-I53_dn5 nanoparticles and all mosaic nanoparticles on a Superose 6 Increase 10/300 GL column.

(E) Reducing SDS-PAGE of individual H1 strains of monohead- and trihead-I53_dn5 nanoparticles and all mosaic nanoparticles, as well as the bare I53_dn5 nanoparticle.

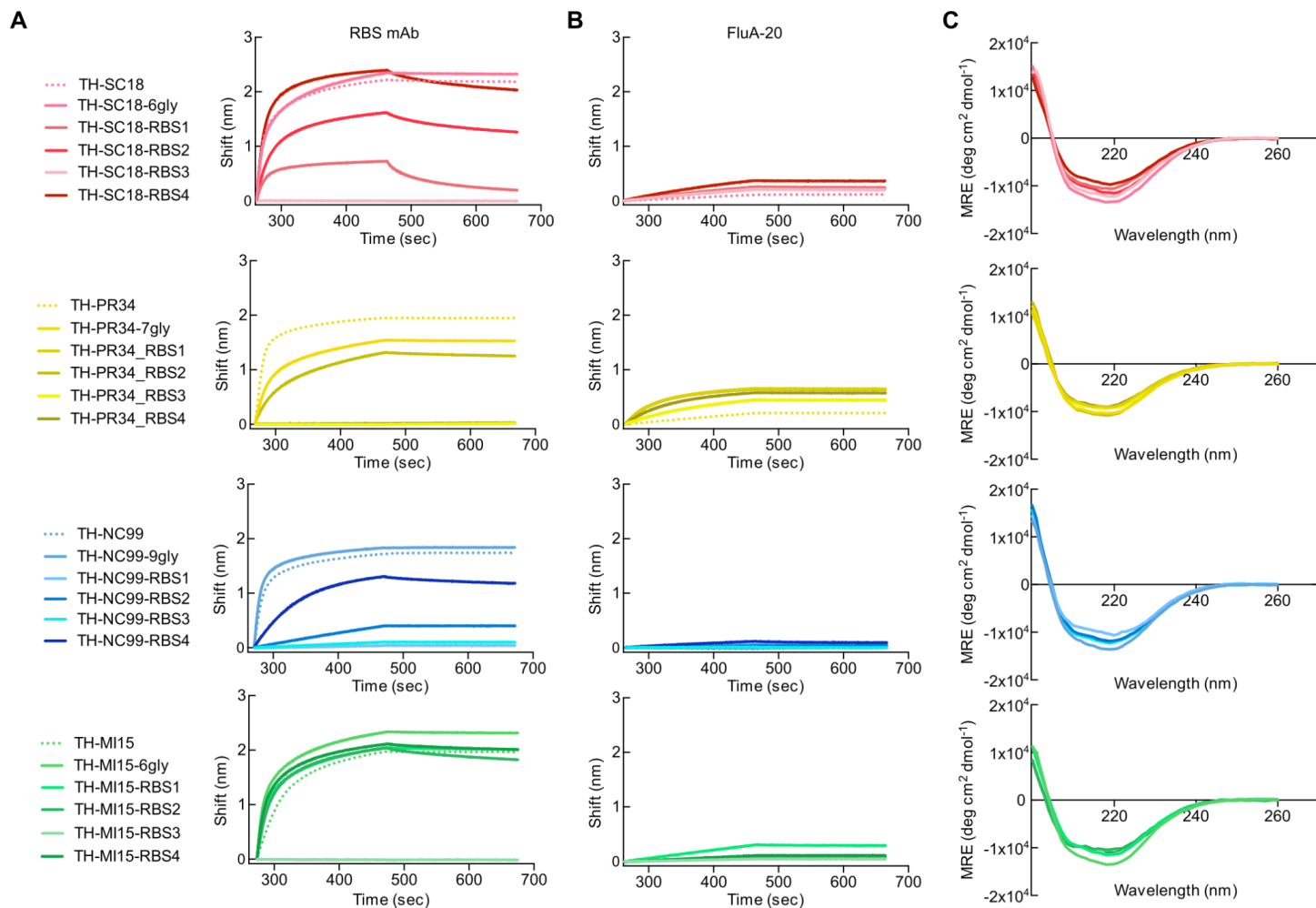(F-G) F. DLS and G. nsEM of all mosaic nanoparticles. Scale bars = 100 nm.

Figure S3 Hypervariable Trihead Immunogen Biophysical Characterization, Related to Figure 3.
(A) Legend of constructs in panels A-C. Binding of RBS-directed mAbs (5J8, anti-PR34, and C05) to all trihead components.
(B) FluA-20 binding to all trihead components.
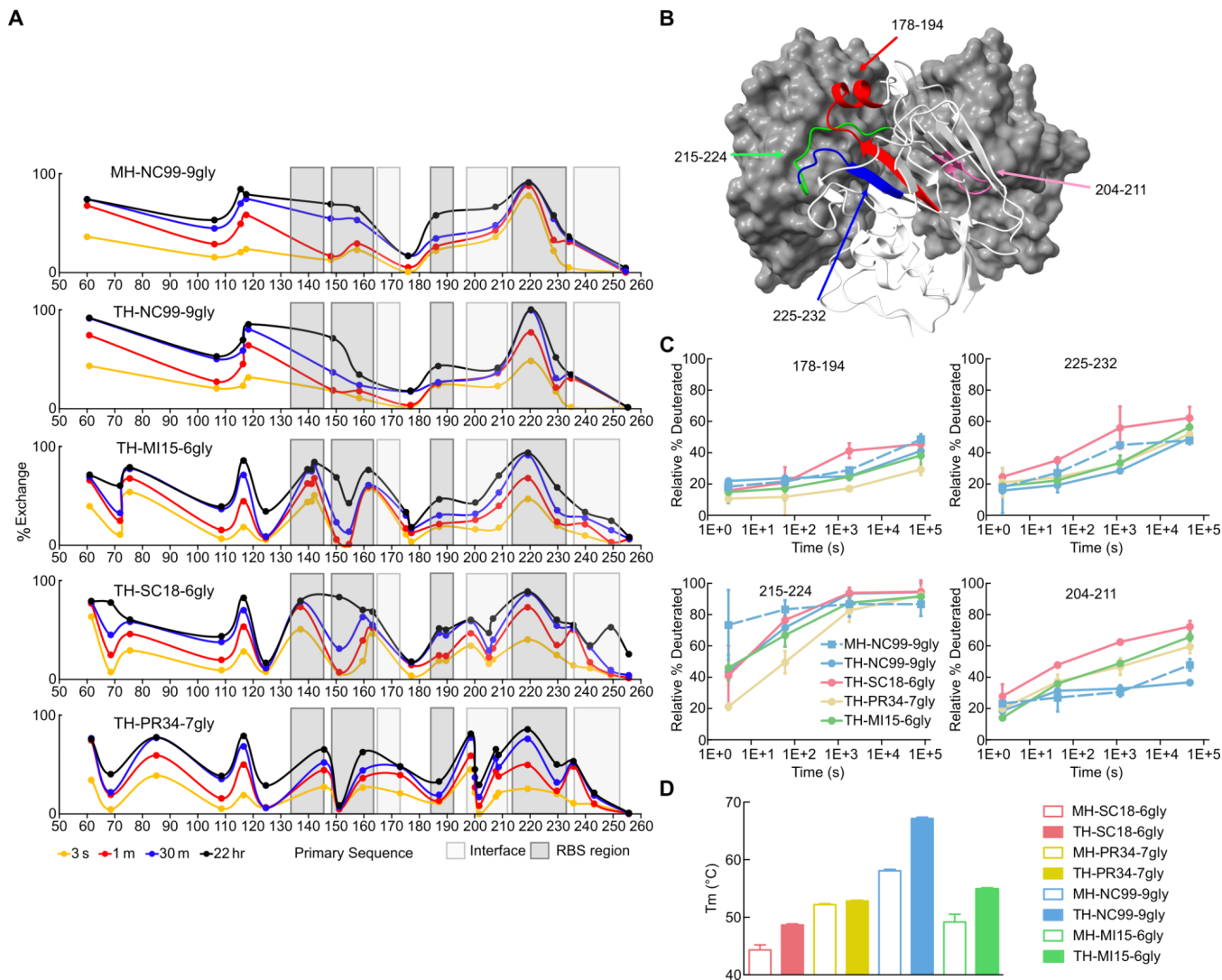(C) Far-UV circular dichroism (CD) spectra of all hypervariable trihead components.

Figure S4 Hyperglycosylated Trihead Stability Characterization by HDX and Thermal Melts, Related to Figure 2.

(A) Deuterium uptake profiles across primary sequence plotted at four different timepoints for each construct.

(B) HDX peptides in panel B highlighted by color on the SI06 (PDB: 5UG0) HA RBD.

(C) Percent deuteration over time for two peptides in the RBS (178-194 and 225-232) and two peptides in the RBD trimer interface (215-224 and 204-211). Each data point represents the mean of biological replicates (n = 3) and the error bars represent ± one SD from the mean.

(D) Melting temperatures of hyperglycosylated monoheads and triheads as measured by NanoDSF. The bars and errors bars represent the mean ± SEM for technical replicates (n = 3).
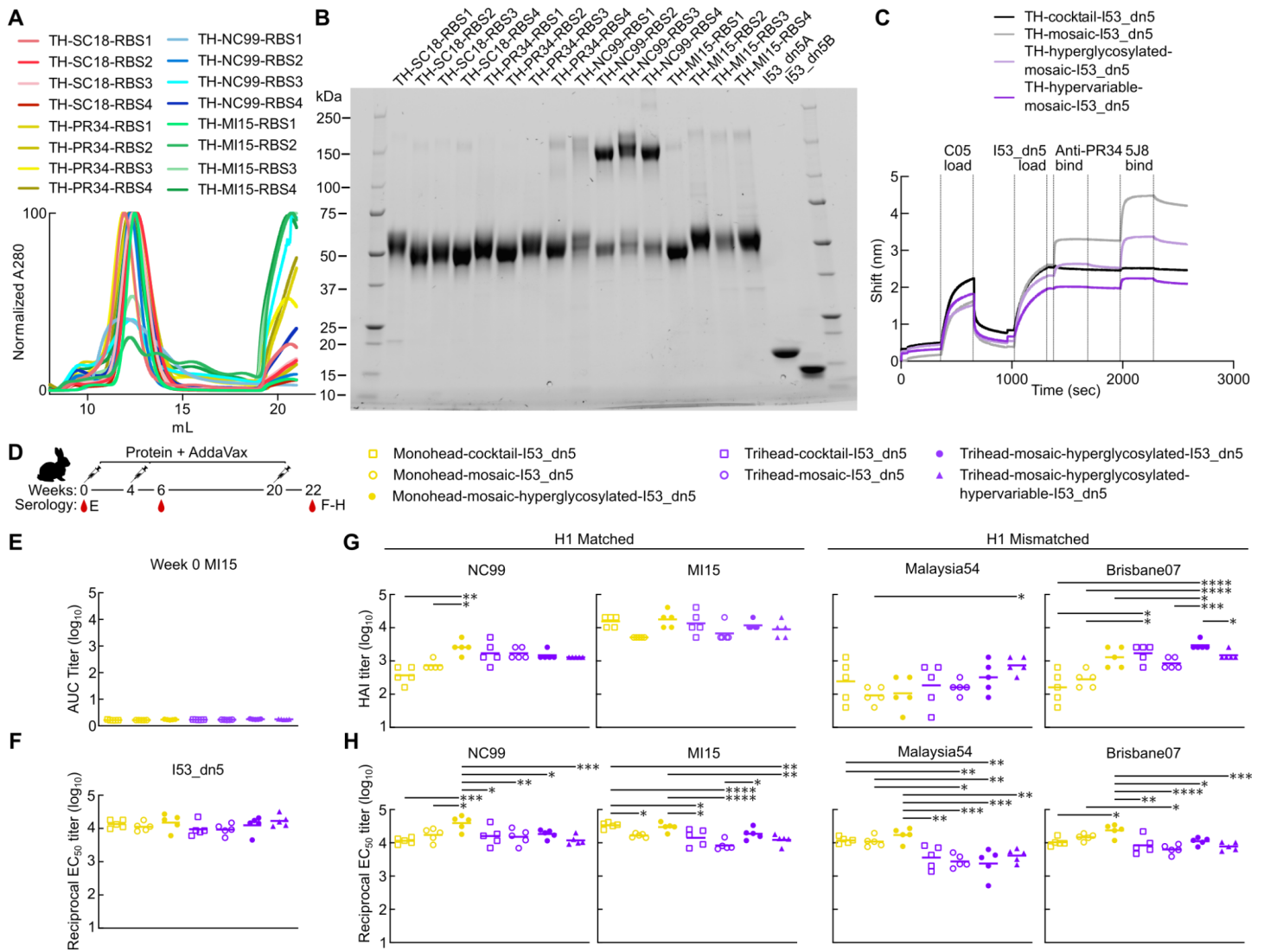
Figure S5 Hypervariable Trihead Immunogen Purification, Mosaic Nanoparticles BLI, and Vaccine-elicited Antibody Responses at Weeks 0 and 22 in Rabbits Immunized with Monohead and Trihead Nanoparticles, Related to Figures 3 and 4.

(A) SEC chromatograms of hypervariable trihead nanoparticle components on a Superdex 200 Increase 10/300 GL column.

(B) Reducing SDS-PAGE of hypervariable trihead-I53_dn5 nanoparticle components, as well as bare I53_dn5B and I53_dn5A nanoparticle components.

(C) Sandwich BLI of trihead nanoparticle immunogens with C05 first captured on AR2G biosensors and then subsequent binding of nanoparticles, anti-PR34, and 5J8.

(D) Hypervariable trihead nanoparticle rabbit immunization schedule and groups.

(E) ELISA binding titers in week 0 serum against vaccine-matched MI15.

(F) ELISA binding titers in week 22 serum against the I53_dn5 nanoparticle scaffold.

(G-H) G. HAI titers and H. ELISA binding titers at week 22, two weeks post second boost.

Each symbol represents an individual animal, and the geometric mean of each group is indicated by the bar (n = 5 rabbits/group). Statistical significance was determined using one-way ANOVA with Tukey's multiple comparisons test; ∗p < 0.05; ∗∗p < 0.01; ∗∗∗p < 0.001; ∗∗∗∗p < 0.0001.

Table S1. Amino acid sequences of novel proteins used in this study, Related to STAR Methods.

Excel Spreadsheet 1.

Table S2. Glycopeptide sequences and occupancies, related to Figure 1, Related to Figure 1.

Construct	Glycopeptide sequence	Sequon	Position	Occupancy (%)
TH-NC99	IAPLQLG**NCS**VAGWILGNPE	G.NCS.V	63	86.6
	NGTCFPGYFADYEE	E.NGT.C	94	99
	ESSWP**NHT**VTGVSASCSHNGK	P.NHT.V	129	99.6
	NGLYP**NLS**K	P.NLS.K	163	45.1
TH-NC99-7gly	IAPLQLG**NCS**VAGWILGNPE	G.NCS.V	63	86.2
	LLI**NAS**SWSYIVET	I.NAS.S	81	46.2
	NGTCFPGYFADYEE	E.NGT.C	94	98.8
	NSSWP**NHT**VTGVSASCSHNGK	K.NSS.W	125b	8.4 single, 91.5 double
		P.NHT.V	129	
	NGLYP**NLS**K	P.NLS.K	163	44.3
	SYVN**NK(S)**	N.NKS.K	171	20.1
TH-NC99-9gly	IAPLQLG**NCS**VAGWILGNPE	G.NCS.V	63	70
	NLSI**NAS**SWSYIVE	C.NLS.I	77	63 single, 37 double
		I.NAS.S	81	
	NGTCFPGYFADYEE	E.NGT.C	94	99.6
	NSSWP**NHT**VTGVSASCSHNGK	K.NSS.W	125b	5.0 single, 95.0 double
		P.NHT.V	129	
	NGLYP**NLS**K	P.NLS.K	163	44.2
	NGLYP**NLS**K**NYT**N**NK(S)**	P.NLS.K	163	49.4 single, 40.8 double, 9.8 triple
		K.NYT.N	167	
		N.NKS.K	171	

Table S3. Mutations introduced into hypervariable trihead antigens, Related to Figure 3 and the STAR Methods.

Trihead RBS variant	Mutations
TH-SC18-RBS1	A144E/S145N/K157S/S159D/T189A/Q192T/S193D
TH-SC18-RBS2	A144M/S145N/S159N/T189E/Q192K/K222E/A227I
TH-SC18-RBS3	A144E/S145D/S159K/T189A/Q192E/S193D/K222Q/ D225N/A227I
TH-SC18-RBS4	S145A/T189E/Q192K/K222E/D225N/A227K
TH-PR34-RBS1	K144Q/S145D/K189S/Q192K/D225G/A227H
TH-PR34-RBS2	E158Q/K189E/Q192T/N193A/K222E/D225G/A227H
TH-PR34-RBS3	E158K/K189N/Q192I/N193S/A227S
TH-PR34-RBS4	Q192H/N193D
TH-NC99-RBS1	G143S/K144V/G189E/R192H/K222A/E227K
TH-NC99-RBS2	K144E/N158G/G159D/G189Q/R192L/A193N/K222V/ E227Q
TH-NC99-RBS3	K144Q/S145L/N158S/R192K/K222V/D225N/E227Q
TH-NC99-RBS4	K144Q/S145L/G189Q/R192L/A193N/D225N/E227H
TH-MI15-RBS1	A142G/G143N/A144V/A189T/Q192M/S193N
TH-MI15-RBS2	A142G/G143N/A144V/N159D/A189K/Q192A/S193T/ K222T/Q225G/G227Q
TH-MI15-RBS3	A144E/K145N/N159S/A189K/Q192M/S193N/K222T/ Q225G/G227Q
TH-MI15-RBS4	A189K/Q192A/S193T